# Quantitative Evaluation of the Hierarchical Porosity in Polyimide Aerogels and Corresponding Solvated Gels

Samantha J. Rinehart<sup>1</sup>, Baochau N. Nguyen<sup>2</sup>, Rocco P. Viggiano<sup>3</sup>, Mary Ann B. Meador<sup>3,\*</sup>, Mark D. Dadmun<sup>1,4,\*</sup>

<sup>1</sup>Department of Chemistry, University of Tennessee, Knoxville, Tennessee 37996
 <sup>2</sup>Ohio Aerospace Institute, 22800 Cedar Point Road, Cleveland, Ohio 44135
 <sup>3</sup>NASA Glenn Research Center, 21000 Brookpark Road, Cleveland, Ohio 44135
 <sup>4</sup>Chemical Sciences Division, Oak Ridge National Laboratory, Oak Ridge, Tennessee 37830

\* Corresponding Authors: <u>Dad@utk.edu</u>; <u>mabmeador@gmail.com</u>

#### Abstract:

Aerogels are promising materials for many aerospace applications, including high performance antennae and flexible insulation because of their inherent low density and high surface areas. Polymer aerogels, especially polyimide aerogels, provide excellent mechanical properties beyond traditional silica aerogels while maintaining the required thermal stability. Polyimide aerogel surface area, porosity, and pore volume are important properties; however, these measurements are traditionally conducted on the aerogel after removal of the solvent. Because of this, the impact of the synthetic control and the solvent presence on the nanoscale to mesoscale structure of polyimide aerogels in functional applications is unclear. In this report, we use small angle neutron scattering to determine the dry and solvated skeletal strut size and composition of polyimide aerogels to deduce the impact of solvation on the structure of complex aerogel struts. Our results show that the aerogel contains a hierarchical assembly of pores, with pores both within and between the supporting struts. This translates to a material with solvent in the larger pores, as well as absorbed in the supporting polyimide skeleton. The amount of solvent uptake in the struts varies with solvent and polyimide properties. The insight from these results provides pathways to determine correlations between aerogel nano- and mesoscale structural characteristics and fabrication processes to their performance in functional applications such as polymeric battery separators. These results also broaden the characterization tools of polymeric aerogels that differentiate between dry and solvated nano- and mesoscale structure that exist in common operating conditions.

### **Introduction:**

Polyimide aerogels are highly porous solids that combine low density, low dielectric constants, and high surface area with excellent mechanical properties<sup>1</sup>. Because of this, they have been demonstrated as thermal insulation for inflatable decelerators and other applications<sup>2,3</sup>, low dielectric substrates for lightweight antennas<sup>4</sup> and triboelectric nanogenerators<sup>5</sup>, and as highperformance filtration devices.<sup>6</sup> Properties of polyimide aerogels have been tailored by use of different backbone chemistry, and different cross-linkers. For example, higher modulus aerogels have been synthesized through the use of more rigid monomers, <sup>7</sup> while more flexible version have been fabricated by the use of diamines with aliphatic spacers.<sup>8</sup> Most recently, polyimide aerogels with improved transparency have been demonstrated through the use of fluorinated diamines and dianhydrides.<sup>9</sup> Cross-linkers used in the synthesis of polyimide aerogels have included 1,3,5triaminophenoxybenzene (TAB)<sup>10</sup>, 1,3,5-triaminophenylbenzene (TAPB),<sup>11</sup> and octaaminopropyl silsesquioxane (OAPS).<sup>12</sup> However, these cross-linkers are quite expensive or not commercially available, and do not tend to direct the properties. Thus, more recently, polyimide aerogels using less expensive and commercially available cross-linkers such as triacid chlorides<sup>13</sup> and triisocyanates<sup>14</sup> have been studied.

Because of their high porosity and good mechanical properties, polyimide aerogels may have application as battery separators for structural batteries. Since polyimides are typically non-flammable, batteries made using polyimide aerogels have potential to improve fire safety of future batteries. Rod-coil block copolyimides have been demonstrated as solid polymer electrolytes, and also as gel electrolytes with room-temperature ionic liquids (RTIL). The use of polyimide aerogels solvated with RTIL rather than less porous polyimides has the potential to improve ionic conductivity as the higher porosity translates to higher RTIL content. These polyimide gel electrolytes may contain up to 95 % RTIL.

RTIL have several important properties which make them well suited as a replacement for current organic electrolytes used in batteries, including improved moisture stability as well as a high degree of ionic conductivity in electrochemical systems. These RTIL share a common structure consisting of a bulky unsymmetrical "onium" organic cation associated with a weakly coordinated organic anion. The most common onium-based cations are 1,3-dialkylimidazolium, N,N-dialkylpyrrolidinium, N,N,N,N-tetraalkylammonium, or N-alkylpyridinium cations.<sup>19</sup> The most popular anion counterparts are: tetrafluoroborate, hexafluorophosphate, bis(tri fluoro methyl sulfonyl) imide, or triflate. The most important properties to consider for selection of RTIL for use as an electrolyte are viscosity, conductivity, diffusion of electroactive solutes, solvation properties, effect of impurities, electrochemical window, and electrochemical stability.<sup>20</sup> Viscosity of the ionic liquid is particularly important in electrochemical studies because it exerts a large impact on the rate of mass transport within the solution and on the conductivity of the salts. RTIL possess viscosities which are 1-3 orders of magnitude larger than conventional liquid electrolytes.<sup>21</sup> The viscosity effect means the ionic conductivities of the RTIL are inversely proportional to the viscosity of the liquid.

RTIL are entirely composed of ions making them among the most concentrated electrolytic fluids possessing numerous charge carriers per unit volume. When these charge carriers are sufficiently mobile, high ionic conductivities are possible despite possessing high viscosities. RTIL exhibit ionic conductivities in the range of 0.1-20 mS/cm, with several members of the imidazolium family exhibiting high ionic conductivities on the order of 10 mS/cm.<sup>22</sup> The imidazolium based ionic liquids were investigated in this research as electrolyte candidates due to their promising combination of relatively low viscosities, high ionic conductivities, a wide electrochemical window, good electrochemical stability, and their inherent non-flammability. The

non-flammable nature of the imidazolium based ionic liquids would enable the development of a safe, non-flammable battery system which could pass the strict aerospace safety standards required for battery systems. By imbibing the imidazolium based electrolyte in a non-flammable polyimide based aerogel film acting as the battery separator, this new separator/electrolyte has two distinct advantages over current state-of-the-art solutions. First, it would possess high ionic conductivity. Second, due to the inherent non-flammability of polyimide aerogels and ionic liquids, the battery would meet safety standards to enable their use in aerospace applications.

The porosity of polyimide aerogels has been characterized using SEM, nitrogen sorptiondesorption and helium pycnometry. However, the porosity of the solvated polyimide gels, before conversion to aerogels, has not yet been characterized. Small angle neutron scattering (SANS) is an extensively used and versatile technique to determine pore connectivity, pore volume fraction, and ratio of open to closed pores within highly porous materials.<sup>22</sup> In this study, we utilize SANS to determine the impact of solvent on the nanostructure and composition of previously reported polvimide aerogels<sup>14</sup> made using 4,4'-oxydianiline, ODA, and biphenyl-3,3,'4,4'-tetracarboxylic dianhydride, BPDA, cross-linked with Desmodur N3300A as shown in Scheme 1. The skeletal struts and pores of the fabricated gels were measured by conducting SANS experiments on both solvent exchanged gels and solvated gels made from dried aerogels. The experimental evidence of the composition and quantitative evaluation of the influence solvent has on the nano and meso scale structures provides a foundation to understanding pivotal interactions within the system that are currently not well-understood. More importantly, application relevant solvents such as RTIL used in battery separator applications were employed to determine structural differences of the gels. Further, the results reported herein broaden the ability to characterize solvated structurally complex materials to develop quantified structure-property relationships and to specifically tailor

both the gel and solvent chemistries to enhance the conductivity of novel polymeric electronic components.

### **Materials:**

ODA was purchased from Wakayama Seika Kogyo Co., Ltd. BPDA was purchased from UBE America, Inc. Desmodur N3300A was obtained from Bayer Material Science. N-methyl pyrrolidone (NMP) was purchase from Tedia, acetic anhydride (AA), trimethylamine (TEA) and bis(trifluoromethane) sulfonamide lithium salt (LiTFSI) were from Sigma-Aldrich. Acetone was purchased from Fisher Chemical. 1-ethyl-3-methylimidazolium bis(trifluoromethyl sulfonyl) imide (IL1), 1-methyl-1-propylpyrrolidiunum bis (trifluoromethyl sulfonyl) imide (IL2) and 1-butyl-1-methylpyrrolidinum bis(trifluoromethyl sulfonyl) imide (IL3) were purchased from IoLiTec, Inc.

### **Experimental:**

Polyimide gels were prepared as shown in Scheme 1 and as previously described<sup>14</sup> with the polyimide backbone formulated to have sixty repeat units between cross-links. To prepare the gels from a 10 wt. % polymer solution, BPDA (6.30 g, 21.4 mmol) in powder form was added to a solution of ODA (4.36 g, 10.9 mmol) in NMP (87.6 ml). Once BPDA was completely dissolved, acetic anhydride (16.2 ml) was added to the solution followed by the addition of trimethylamine (6.0 ml). The mixture was once again stirred until a homogeneous solution was obtained. Finally, Desmodur N3300A (0.1200 g, 0.238 mmol) was then added to the mixture to cross-link the polymer chains. The polymer solution was poured into a 2 mm thick closed mold. Gelation occurred within ten minutes. The resulting polyimide gel was aged at room temperature for one day before being extracted into a mixture of 50:50 vol/vol of NMP/acetone, followed by subsequent washes of 100 vol% acetone twice daily to completely remove any residual NMP.

$$(n) + (n+1) \underset{H_2N}{\overset{\circ}{\bigvee}} + (n+1) \underset{H_2N}$$

**Scheme 1**. Synthesis of polyimide gels based on 4,4'-oxydianiline (ODA), biphenyl-3,3,'4,4'-tetracarboxylic dianhydride (BPDA), and cross-linked using Desmodur N3300A.

Some of the polyimide gels were dried through a supercritical extraction technique in which the acetone residing in the pore network was replaced with liquid  $CO_2$  under pressure. Supercritical extraction occurs by first heating the system, which forces  $CO_2$  into a supercritical state, eliminating liquid vapor pressure and driving  $CO_2$  out of the pore structure. This results in converting the wet gel into the dry aerogel state. To ensure that the solvent has been completely removed from the aerogel structure, the samples are dried in a vacuum oven at 75 °C overnight. Once dried, the aerogels were characterized to obtain their density, porosity, average pore size, and total surface area. The bulk density  $(\rho_b)$  is the sample weight divided by the volume which is calculated from width, length and thickness of the sample. The skeletal density  $(\rho_s)$  was measured using a Micromeritics Accupyc 1340 helium pycnometer. The porosity is calculated as shown in

Eq. 1. The Brunauer–Emmett–Teller surface area analysis and pore distribution were computed using a Micromeritics ASAP 2020 chemisorption apparatus.

% Porosity = 
$$(1-\rho_b/\rho_s) \times 100$$

Equation 1

Scanning electron microscopy (SEM) images were taken using a Hitachi S-4700-II microscope.

To prepare for the small angle neutron scattering (SANS) experiments, polyimide gels were immersed in water or D<sub>2</sub>O at room temperature. The aerogel specimens sank to the bottom of the jars indicating they were fully imbibed with solvent. Other gels were prepared by solvent exchanging the acetone containing gels by soaking them in water or D<sub>2</sub>O. A similar solvent exchange process was used to imbibe wet gels with one of three separate electrolytes. The electrolytes were prepared first by dissolving 10 wt.% of Lithium Trifluoromethanesulfonimide (LiTFSI) as the lithium salt to 3 separate ionic liquids (IL), identified as IL-1: 1-ethyl-3-methylimidazolium bis(trifluoromethyl sulfonyl) imide, IL-2: 1-methyl-1-propylpyrrolidiunum bis (trifluoromethyl sulfonyl) imide, IL-3: 1-butyl-1-methylpyrrolidinum bis(trifluoromethyl sulfonyl) imide.. This procedure was performed in a dry room to prevent the absorption of water moisture. Complete removal of acetone in the IL/LiTFSI solvated polyimide gels was confirmed via thermal gravitational analyses (TGA) shown in Figure 1. TGA was performed under N<sub>2</sub> gas. The plot of weight % vs. temperature shows only a 0.5 wt.% weight loss occurring from 135 °C to 325 °C before the onset of decomposition at 370 °C.

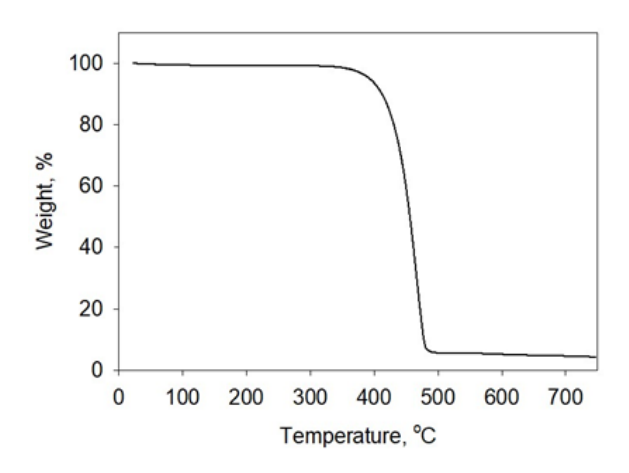


Figure 1: TGA curve of [EMIM][TFSI] with 10 wt.% LiTFSI.

Small angle neutron scattering (SANS) experiments were conducted on aerogels and solvated polyimide gels at the National Institute for Standards and Technology's Center for Neutron Research (NCNR) using the NG-7 beamline and the High Flux Isotope Reactor at Oak Ridge National Laboratory on the GP-SANS beamline. Three separate detector distances provided a Q range of 0.001 to 0.55 Å<sup>-1</sup>, where Q is the wave vector equal to  $(4\pi/\lambda)(\sin(\theta/2))$ , where  $\lambda$  is the neutron wavelength, and  $\theta$  is the scattering angle. Each polymeric aerogel sample was placed in a 2 mm sample holder between two quartz windows. For the solvated polyimide gels, the samples were immersed in protonated, deuterated, or a contrast matched solvent for several hours overnight until equilibrium was reached. Once the aerogel samples were assembled in the sample holder, the solvent was added. All raw data was normalized to detector sensitivity, empty cell, and detector dark current.

# **Results and Discussion:**

The aerogel formulation prepared for this study had a density of 0.185 g/cm<sup>3</sup> and a porosity of 87 % as a result of 24 % shrinkage during processing. This is similar to previously reported aerogels made using ODA and BPDA and cross-linked with Desmodur N3300.<sup>14</sup> Brannuer

Emmet-Teller (BET) analysis of nitrogen sorption gave a surface area of  $344 \text{ m}^2/\text{g}$ , also similar to previously reported polymer aerogels from that study using 10 wt. % polymer concentration . The pore size distribution and a scanning electron micrographs (SEM) cross section of the aerogel are shown in Figure 2. The pore size distribution in Figure 2a shows a broad pore size distribution centered at 11-25 nm, and has a small, but notable peak at 3-4 nm. The SEM in Figure 2b is typical for polyimide aerogels and is also similar to those reported previously.  $^{14}$ 

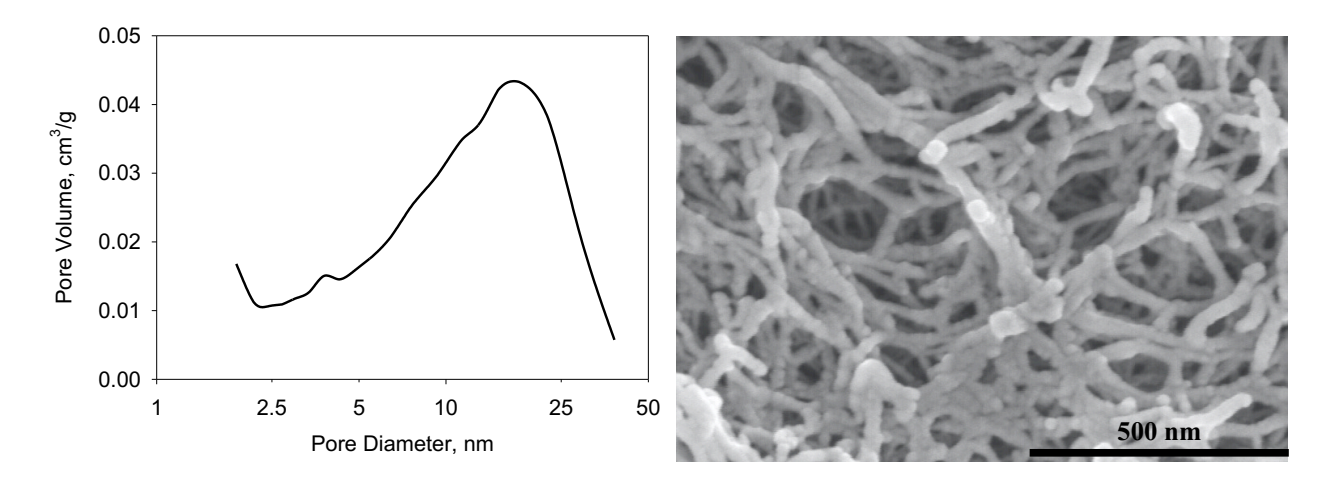


**Figure 2.** The pore size distribution comparing the pore diameter to pore volume and SEM of the aerogel.

Small angle neutron scattering (SANS) provides information on the morphology, composition, and density of polymeric materials.<sup>23</sup> SANS is a versatile technique that permits determination of the structure of the aerogels and solvated polyimide gels.<sup>24,25,26,27</sup> Moreover, the impact the introduction of solvent has on the polyimide network (pores and struts) (in the presence or absence of solvent) can be monitored. Solvent exchange, where the solvent used for synthesis is directly replaced with a solvent of interest, is one fabrication method studied, where the other is a process where the aerogels are super-critically dried and then re-solvated with the solvent of interest. Throughout this manuscript, the samples that are super critically dried prior to the reintroduction of a solvent will be referenced as solvated SCD-gels, while the solvent exchanged

samples will be referenced as solvated SE-gels. The ability to study solvent imbibed polymeric materials provides information critical for correlating multi-length scale structure and composition to performance; a crucial requirement for polyimide aerogels used as battery separators where the ionic conductivity is monitored in various ionic liquid environments.

# The structure and composition of hydrated polyimide gels

SANS experiments of the polyimide aerogel, D<sub>2</sub>O solvated SCD-gels, and the H<sub>2</sub>O or D<sub>2</sub>O solvated SE-gels were completed and the reduced SANS curves are provided in Figure 3. Qualitatively, each processing and solvent environment shows various scattering intensities across the entire q-range. The aerogel exhibited the strongest scattering intensity at low-q and the D<sub>2</sub>O solvated SE-gel had the weakest scattering intensity. The intensity of scattering is a function of the size of the scattering object and the degree of scattering contrast present between the polyimide gel and the solvent.<sup>23,28,29</sup> Most likely, the solvated samples all have lower scattering intensities due to the scattering length density of the solvent being greater than that of air (which is 0). This results in a greater scattering contrast for the aerogel sample than for the solvated gel.<sup>29,30</sup>

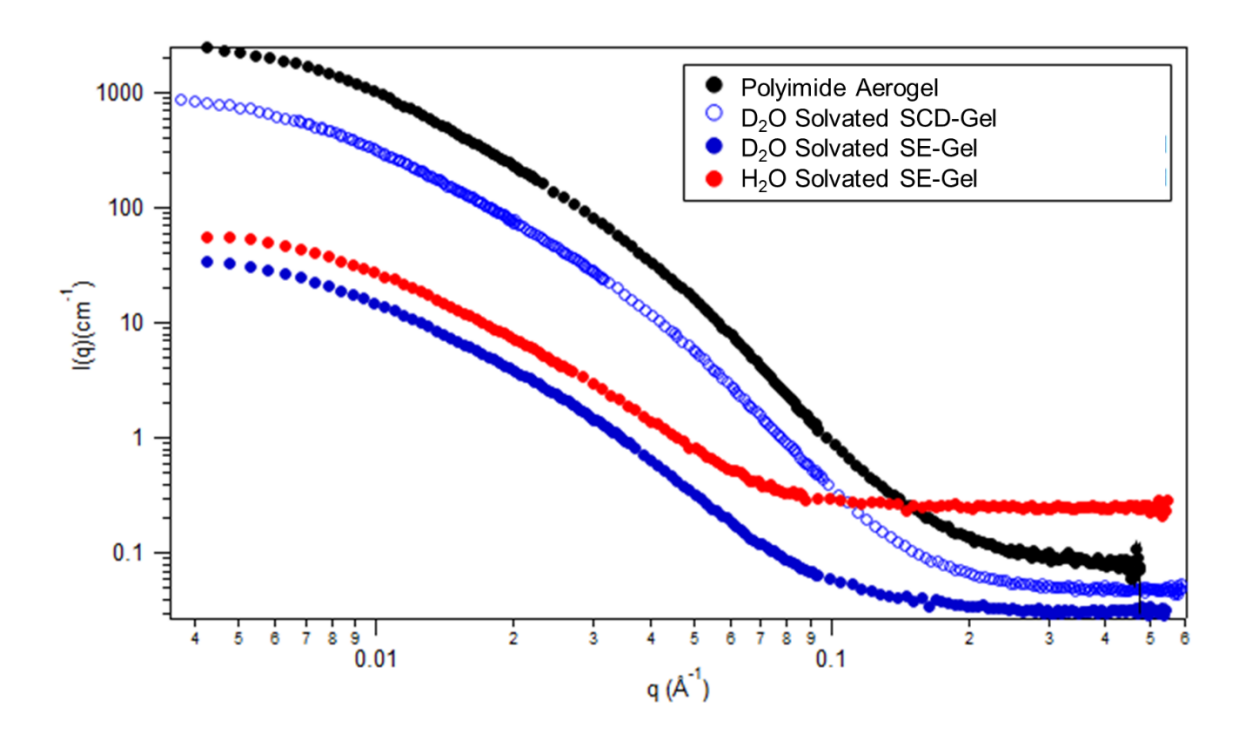


**Figure 3.** Small angle neutron scattering curves of the aerogel (black) and D<sub>2</sub>O solvated SCD-gels (blue open circles), D<sub>2</sub>O solvated SE-gels (blue closed circles) and s H<sub>2</sub>O solvated SE-gels (closed circles red).

To accurately analyze the scattering curves to determine the structure and composition of the solvated gels, the volume fraction of polyimide in the sample is needed. This was determined using the transmission of the aerogel and Equation 1, which defines the relationship between the volume fraction of aerogel,  $f_A$ , the absorption coefficient of the aerogel [ $\mu_A$  (cm<sup>-1</sup>)], and of the solvent (or air) [ $\mu_S$  (cm<sup>-1</sup>)], the measured transmission, T, and the sample thickness, t (cm). In this equation,  $I_{tr}$  and  $I_0$  are the transmitted beam intensities after and before the sample, respectively.<sup>31</sup> The absorption or attenuation coefficient of the polymer and the solvent can be calculated using the NCNR SLD calculator or experimentally obtained with Equation 2 when the transmission and thickness of pure component is measured. The experimentally obtained polymer properties from this analysis are summarized in Table 1.

$$T = \frac{I_{tr}}{I_0} = \exp\left[-t\{\mu_A f_A + \mu_S (1 - f_A)\}\right]$$
 Equation 2

$I = \frac{I_{tr}}{I_{s}} = I_{s}$	$\exp(-\mu t)$	Equation 3
10		

**Table 1.** Experimentally obtained properties of the polyimide aerogel.

T

Neutron Transmission of aerogel	0.854
Aerogel Thickness (cm)	0.171
Experimentally Measured Linear Attenuation Coefficient (μ) (cm <sup>-1</sup> )	0.923
Calculated Linear Attenuation Coefficient (μ) (cm <sup>-1</sup> )	2.49
Calculated Aerogel Volume Fraction	0.37

The experimentally obtained polymer volume fraction is 0.37 which is inconsistent with the porosity characterization of the aerogel (aerogel volume fraction  $\sim 0.13$ ). It is important to emphasize that 0.37 denotes the volume fraction of the polyimide aerogel in the sample cell, not necessarily the volume fraction that is associated with the porosity. The volume fraction of the polyimide aerogel in the sample cell is used within an appropriate model to extract the structure and composition of the solvated gels. The scattering model applied to the polyimide gel scattering curves is the cylinder model by Guinier and Fournet.<sup>32</sup> This model provides a form factor for a right circular cylinder normalized for all possible orientations of the cylinder. 33,34 Many other fitting models were tested during the analysis of these gels yet the cylinder model proved most reliable for these systems. The reliability of the cylinder model indicated that the scattering of the aerogel struts dominated, and the aerogel junctions can be neglected. The scattering length densities (SLD) of the polyimide aerogel  $(3.41\times10^{-6} \text{ Å}^{-2})$ , air  $(0 \text{ Å}^{-2})$ , water  $(-0.56\times10^{-6} \text{ Å}^{-2})$ , and deuterium oxide (6.39×10<sup>-6</sup> Å<sup>-2</sup>) were calculated with the NCNR SLD calculator using the chemical compositions and densities shown in Table 2. The volume fraction (0.37) and corresponding solvent SLD were held constant and the fitting software SasView was used to fit to

the cylinder model which provides the cylinder radius, polydispersity of the radius, cylinder length, length polydispersity, and cylinder SLD. Figure 4 shows the resultant fit for the scattering of the polyimide aerogel with excellent agreement over the entire Q-range.

**Table 2.** Composition and density of materials studied.

	Polyimide Aerogel	Water	Deuterium Oxide
<b>Chemical Composition</b>	$C_{28}N_2O_5H_{14}$	H <sub>2</sub> O	$D_2O$
Density (g/mL)	1.38	1.00	1.11
Scattering Length Density	3.30×10 <sup>-6</sup> Å <sup>-2</sup>	-0.56×10 <sup>-6</sup> Å <sup>-2</sup>	6.39×10 <sup>-6</sup> Å <sup>-2</sup>

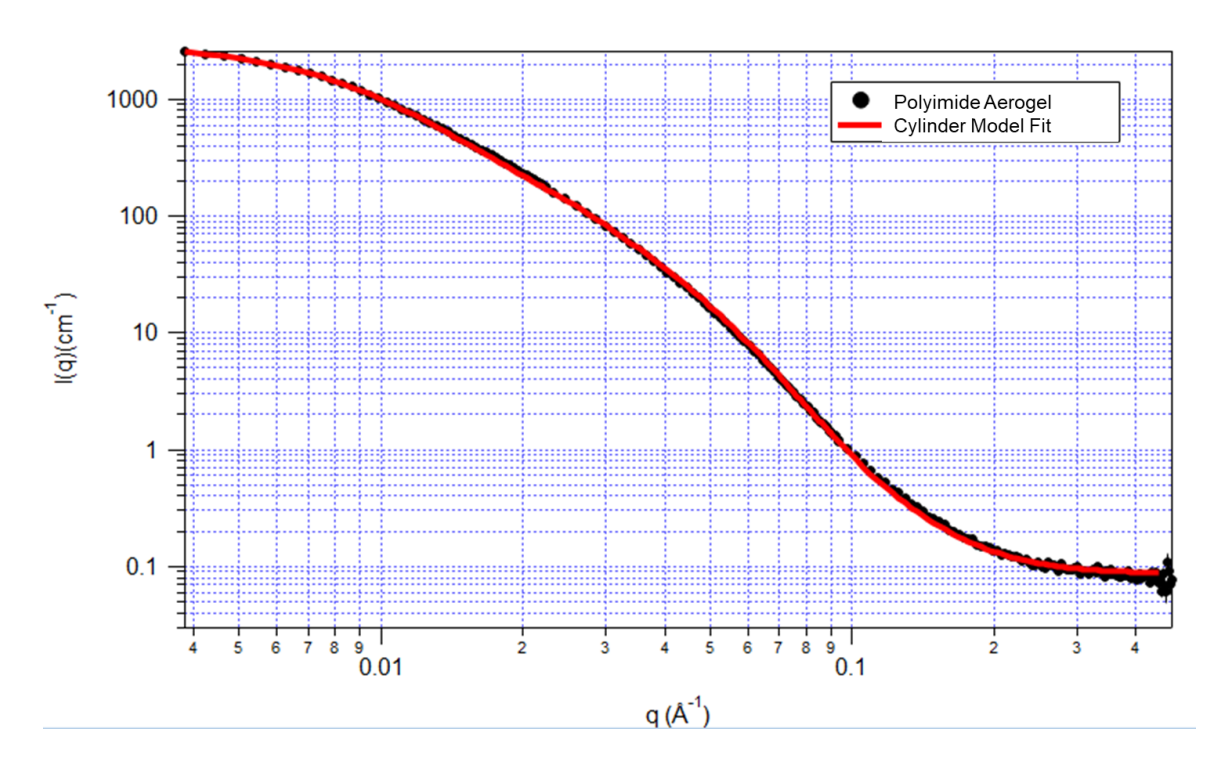


**Figure 4.** The small angle neutron scattering curve for the polyimide aerogel (black circles) fit with the cylinder model (red line).

The cylinder is structurally interpreted as the size and composition of the polymeric strut of the aerogel. The polydispersity of the cylinder radius is described with a Schulz distribution. The distribution of the cylinder radii based on this model is provided in Figure 5 for all solvated

gels (critically dried or solvent exchanged) and the aerogel. The mean radii for the struts in the solvent exchanged gel are 196 Å and 204 Å for the  $D_2O$  and  $H_2O$  samples, respectively. The  $D_2O$  solvated SCD-gel exhibits a slightly smaller mean radius of 180 Å while the aerogel struts sans solvent have a mean radius of 182 Å. The size of the aerogel strut correlates the structure of the formed aerogel to its processing, where the radius of the strut that underwent critical drying prior to reintroduction of solvent is smaller than that of the solvent exchanged gels by approximately 2 nm.

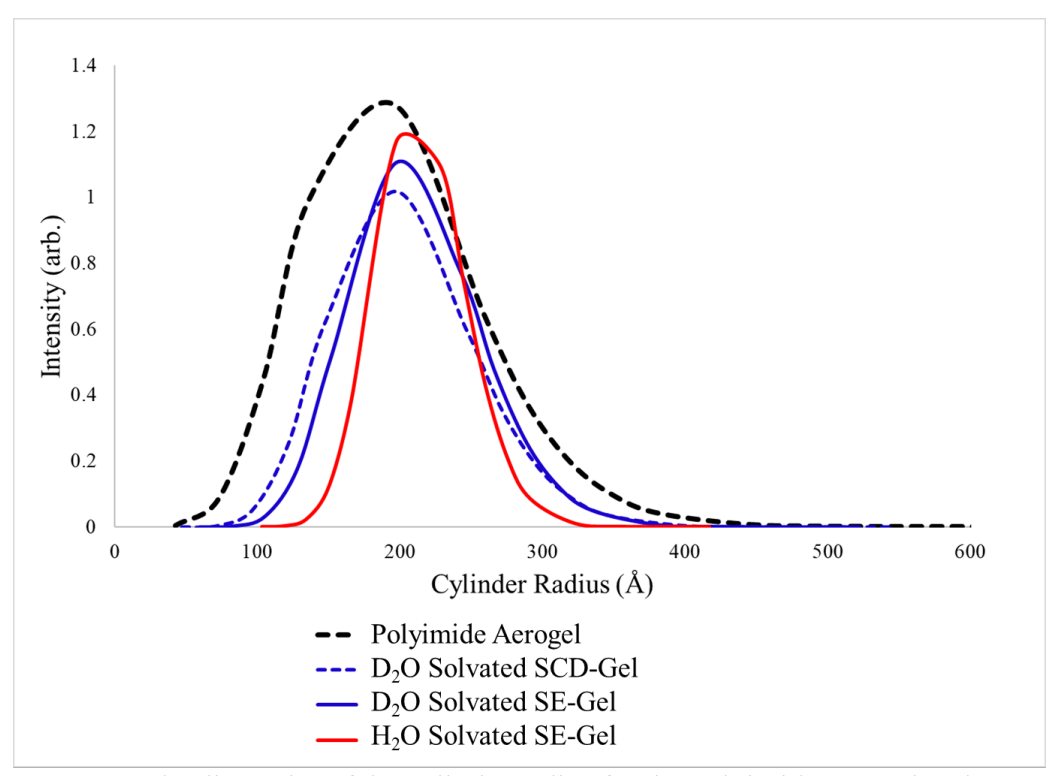


**Figure 5.** The dispersity of the cylinder radius for the polyimide aerogel and H<sub>2</sub>O and D<sub>2</sub>O solvated SCD-gels and SE-gels derived from the cylinder model fit.

The cylinder model also provides a measure of the scattering length density (SLD) of the strut, which is related to its composition. The SLD contrast between that of the pure solvent (or air) in the pores and the SLD of the polyimide strut defines the intensity of the scattering. Table 3 lists the calculated scattering length density contrast between the polyimide strut and the solvent

(assuming the strut is pure polyimide) and the experimentally measured SLD contrast between the pore and the aerogel strut. Inspection of this table shows that the SLD contrast observed experimentally in the solvated samples is less than the values calculated for the pure polyimide strut. This discrepancy can be explained by the fact that the polyimide strut is not comprised of pure polyimide, rather is swollen with the solvent. In other words, the strut is comprised of a mixture of solvent and polyimide.

**Table 3.** The calculated and experimentally measured contrast between the solvent or air and the cylinder (polyimide strut) for each sample combination.

Sample	Calculated SLD Contrast (×10 <sup>-6</sup> Å <sup>-2</sup> )	Experimentally Measured SLD Contrast (×10 <sup>-6</sup> Å <sup>-2</sup> )
Aerogel	3.41	2.61
Solvated SE-Gel H <sub>2</sub> O	4.00	0.50
Solvated SE-Gel D <sub>2</sub> O	2.90	0.35
Solvated SCD-gel D <sub>2</sub> O	2.90	1.55
Contrast Match Solvated Polyimide Gel	0.00	0.02

The SLD contrast depends on an accurate measure of the scattering length density of the pure polyimide, which was verified with a contrast matching experiment.  $^{23,30,33}$  The SLD of the polyimide aerogel is calculated to be  $3.41\times10^{-6}$  Å $^{-2}$  based on the chemical composition and measured density of the aerogel. A 42/58 mixture of H<sub>2</sub>O and D<sub>2</sub>O has a similar SLD; and the scattering of the polyimide gel in this mixed solvent was measured and is included in Figure 6. The reduced scattering intensity across the entire q-range of the contrast matched small angle scattering curve indicates there are no closed pores, all pores are filled with solvent,  $^{23,30,35}$  and verifies the accuracy of the calculated SLD of the polyimide.

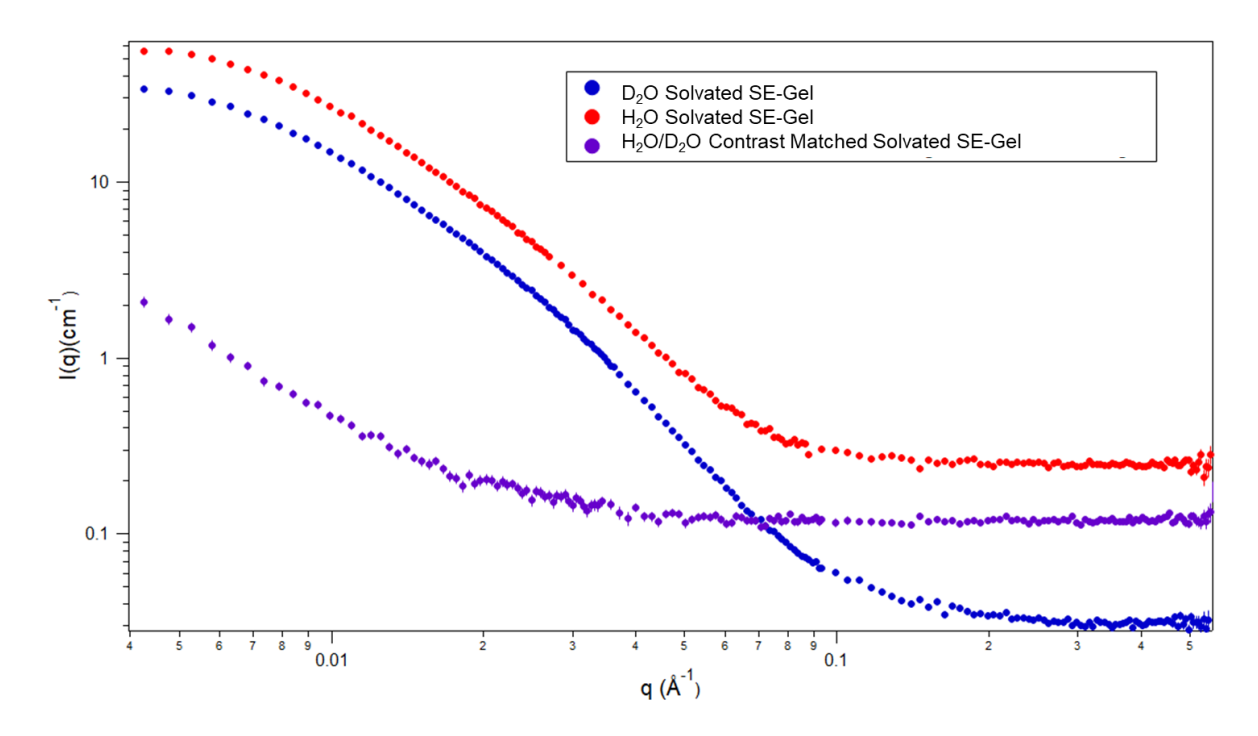


**Figure 6.** The reduced scattering curves of polyimide gels solvated in water (red), deuterium oxide (blue), and a contrast matched solution (purple).

The reduced experimental scattering length density contrast between the polyimide aerogel and its solvent, air (Table 3) indicates that not only is air found in the open pores of the aerogel, but the aerogel struts must contain additional open pores. Of course, the pores in the aerogel strut may also imbibe solvent, and therefore Equation 3 was employed to determine the volume fraction of solvent in the aerogel strut ( $\phi_{solvent\ in\ strut}$ ). In Equation 3, SLD<sub>cylinder</sub> is the experimentally obtained SLD of the polyimide strut (listed in Table 4), SLD<sub>polyimide</sub> is the theoretically calculated SLD of the polyimide (verified by the contrast match experiment), and SLD<sub>solvent</sub> is the SLD of solvent, or in the case of the aerogel, air.

$$\frac{SLD_{cylinder} - SLD_{polyimide}}{SLD_{solvent} - SLD_{polyimide}} = \phi_{solvent \ in \ strut}$$
 Equation 3

**Table 4.** The experimentally measured SLDs from the cylinder model fit\* and the contrast matched experiment.

	Scattering Length Density (x10 <sup>-6</sup> Å <sup>-2</sup> )
Cylinder (Polyimide Aerogel No Solvent)	2.61
Cylinder (D <sub>2</sub> O Solvated SE-Gel)*	5.95
Cylinder (D <sub>2</sub> O Solvated SCD-Gel)*	4.75
Cylinder (H <sub>2</sub> O SE-Gel)*	-0.08
D <sub>2</sub> O	6.33
H <sub>2</sub> O	-0.59
Polyimide	3.41

The calculated volume fraction of solvent in the strut are provided in Figure 7 based on these calculations. These data show that the D<sub>2</sub>O solvated SCD-Gel has the smallest fraction of solvent in the struts with 49%, while the D<sub>2</sub>O and H<sub>2</sub>O solvated SE-Gels have the a much larger volume fraction of solvent in the struts at 88%. The extensive uptake of water by these gels is consistent with previous studies that show aerogel formulations with ODA as the diamine readily uptake water, but that the moisture resistance of the gel can be improved with variation in diamine structure.<sup>7</sup> The dotted line on Figure 7 represents the porosity of the polyimide strut in the aerogel calculated from Equation 3. Since the volume fraction of solvent in the struts of all the solvated samples are larger than the aerogel strut porosity, this indicates that the struts adsorb solvent beyond the fraction of pores within the strut. This solvent absorption is consistent with an increase in the radius of the cylinders by 2 nm when the gels are solvent exchanged rather than super critically dried.

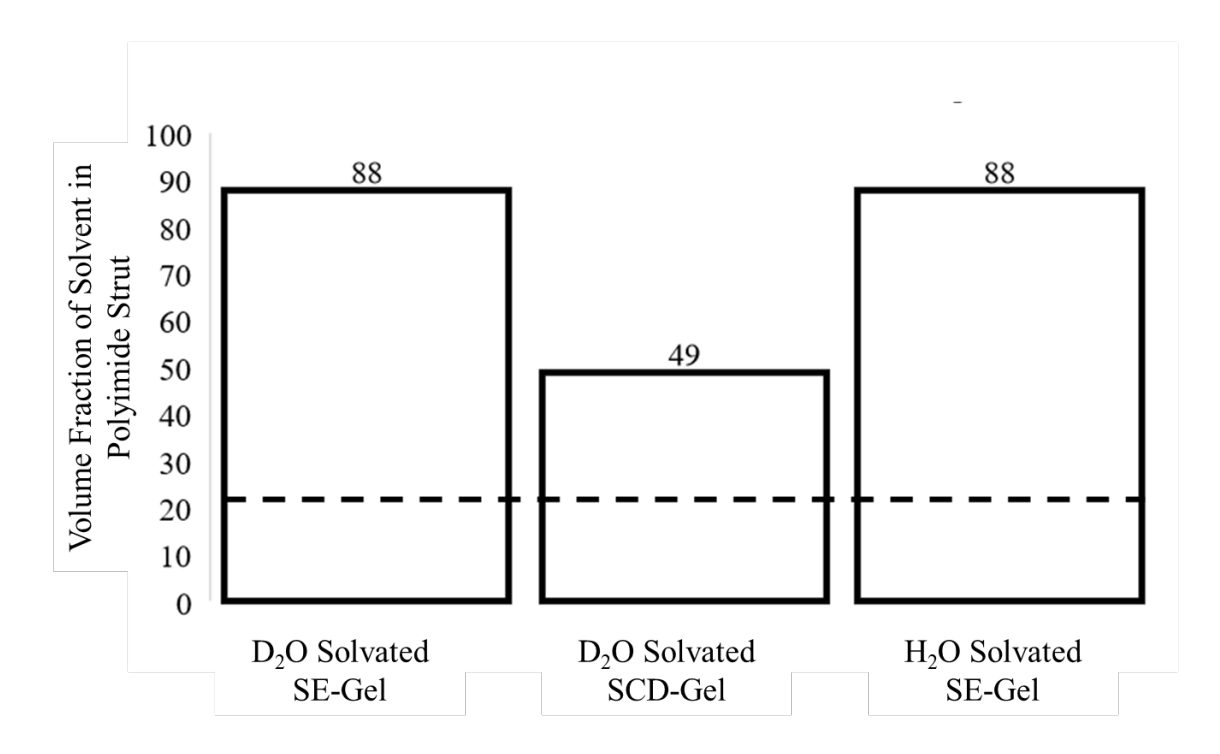


**Figure 7.** The volume fraction of H<sub>2</sub>O or D<sub>2</sub>O Solvated Polyimide Gel struts. The dashed line represents the porosity of the Polyimide Aerogel strut.

Summarily, these analyses show that the aerogels contain ~21% pores within the strut and when solvated, all pores within the polyimide strut become filled. Additionally, the polyimide gel struts swell significantly beyond the dry strut porosity. The hierarchical pore size distribution is consistent when quantitatively comparing the structure and composition of the scattering of a series of solvated SE-Gels with varying degrees of contrast, an aerogel, and a solvated SCD-gel. Moreover, the presence of the porosity within the aerogel strut has not been previously identified, though is consistent with a slight bimodal distribution of pores observed in BET measurement. 36,37,38

Of even more importance is that this hierarchical structure of the porosity may impact the performance of the aerogels as a functional material. For instance, there is interest in using porous polyimides as battery separators, which require transport of ions through the aerogel. The presence of the smaller pores within the struts may provide additional channels for transport or additional

tortuosity to ion transport. With this in mind, the structure of 4,4'-oxydianiline (ODA) based polyimide aerogels solvated with three ionic liquids were determined by similar small angle neutron scattering experiments. These samples were fabricated by solvent exchange.

# Aerogels Solvated with Application Relevant Solvents

The nanostructure of each polyimide gel was investigated when solvated with three ionic liquids. Each ionic liquid had the same anion (CF<sub>3</sub>SO<sub>2</sub>)<sub>2</sub>N<sup>-</sup>, but varying cations: 1-ethyl-3-methylimidazolium bis(trifluoromethyl sulfonyl) imide (Ionic Liquid 1 or IL1), 1-methyl-1-methylpyrrolidiunum bis (trifluoromethyl sulfonyl) imide (Ionic Liquid 2 or IL2) and 1-butyl-1-methylpyrrolidinum bis(trifluoromethyl sulfonyl) imide (Ionic Liquid 3 or IL3).

SANS experiments were conducted of the polyimide aerogel and solvated with each ionic liquid as SE-Gels. The SANS curves for the polyimide aerogels and solvated SE-gels are provided in Figure 8. Qualitatively, the aerogel has the strongest low q scattering intensity while the solvated aerogels all have reduced, yet similar I(0) scattering intensities. As in the H<sub>2</sub>O and D<sub>2</sub>O samples above, the dry aerogel scatters the strongest, because it has the largest scattering density contrast between polyimide and empty pore.

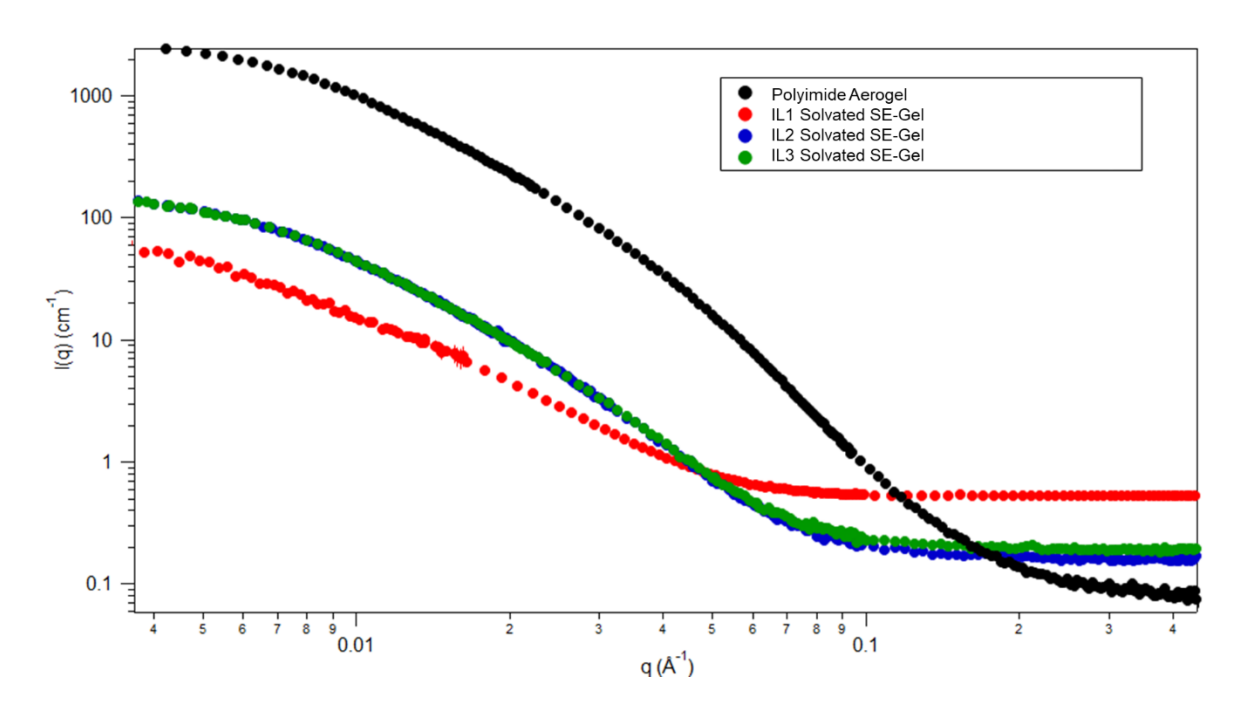


**Figure 8.** Small angle neutron scattering curves of the polyimide aerogel and solvated SE-Gels with each ionic liquid.

The volume fraction of the pores within the aerogel was determined by the described procedure above, which shows that the porous volume fraction is 0.20. The compositions, densities, and scattering length densities (SLDs) of the three ionic liquids are provided in Table 5. As above, the data were fit to the cylinder model using SasView to provide the cylinder radius, polydispersity of the radius, cylinder length, length polydispersity, and cylinder SLD.

**Table 5.** Compositions, densities, and SLDs of the three ionic liquids used.

	Ionic Liquid 1	Ionic Liquid 2	Ionic Liquid 3
Composition	$C_8H_{11}N_3F_6S_2O_4$	$C_{10}H_{18}N_2F_6S_2O_4$	$C_{11}H_{20}N_2F_6S_2O_4$
Density (g/mL)	1.53	1.44	1.40
Scattering Length Density	2.42×10 <sup>-6</sup> Å <sup>-2</sup>	1.71×10 <sup>-6</sup> Å <sup>-2</sup>	1.59×10 <sup>-6</sup> Å <sup>-2</sup>

The polydispersity of the polyimide cylinder radius is described with a Schulz distribution and is shown in Figure 9. The mean radius for the ionic liquid solvated SE-Gels ranges from 20.8 - 23.9 nm while the mean radius of the polyimide aerogel strut is 19.7 nm. There is a small shift

in the cylinder radius in the SE-Gels, where the cylinder of the samples solvated with ionic liquid 1 and 3 are less than the cylinder radius of the SE-Gel solvated with ionic liquid 2.

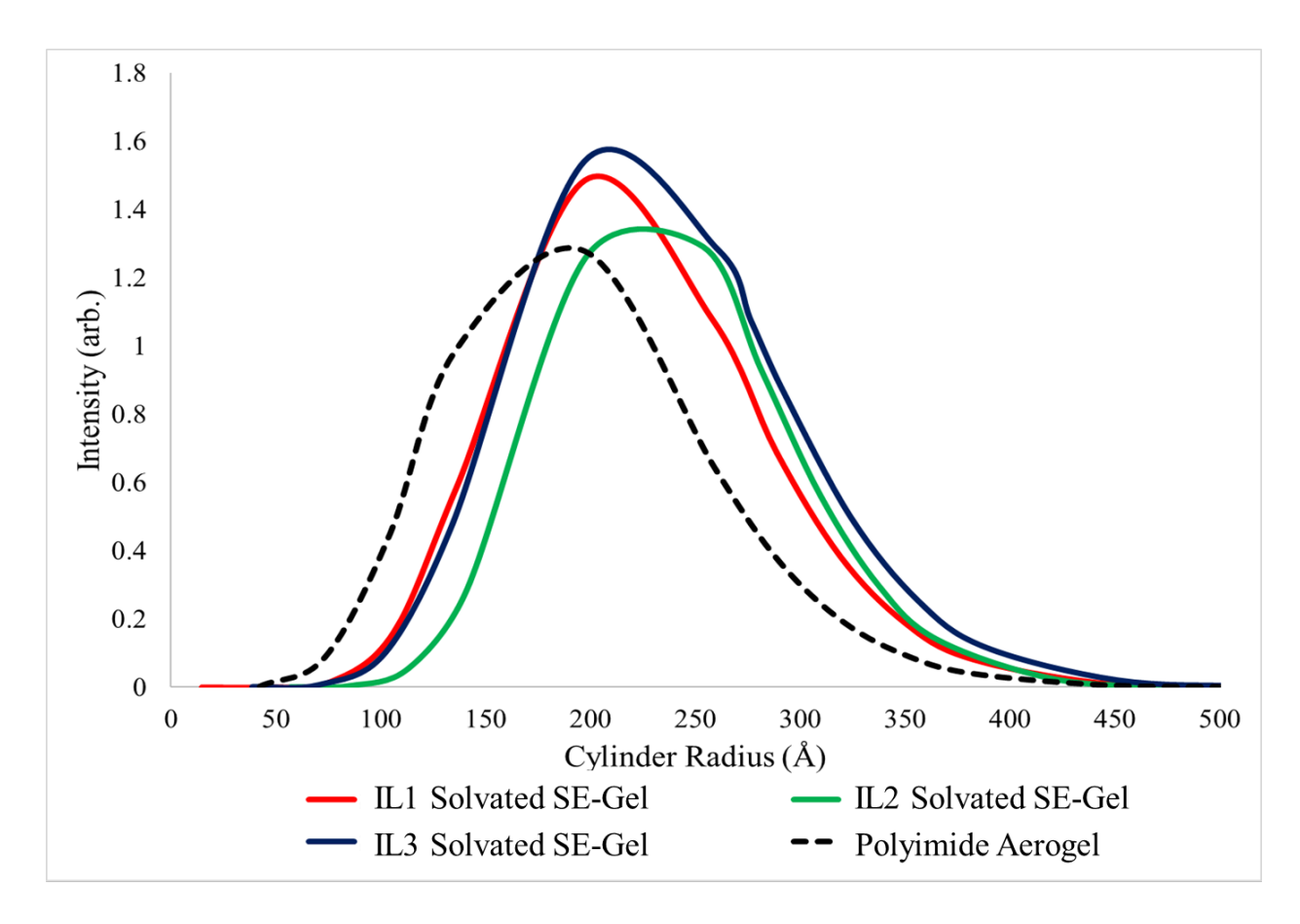


**Figure 9.** The Schulz distribution of the cylinder radius for the polyimide aerogel and ionic liquid solvated SE-Gels derived from the cylinder model fit.

As with the SE-Gels solvated with H<sub>2</sub>O and D<sub>2</sub>O, the cylinder model used throughout this analysis provides a SLD contrast between the cylindrical scattering object (i.e. the polyimide strut) and the solvent. The contrast matching experiment previously described in this manuscript confirms the polyimide aerogel SLD as 3.41x10<sup>-6</sup> Å<sup>-2</sup> and that all of the pores are filled with solvent. However, the calculated SLD contrast of each sample is inconsistent with the experimentally measured SLD contrast, shown in Table 6. The discrepancies between the

calculated and experimentally measured SLD contrasts is explained by the pores filling with ionic liquid as well as the polyimide struts absorbing ionic liquid.

**Table 6.** The theoretically and experimentally measured contrast between the solvent or air and the cylinder (polyimide strut) for each sample combination.

	Theoretical	Experimentally
Sample Polyimide Aerogels	SLD	Measured
	Contrast	SLD Contrast
	$(\times 10^{-6} \text{ Å}^{-2})$	$(\times 10^{-6} \text{ Å}^{-2})$
Polyimide Aerogel	3.30	2.61
IL1 Solvated SE-Gel	0.88	0.34
IL2 Solvated SE-Gel	1.59	0.52
IL3 Solvated SE-Gel	1.71	0.52

To quantify the amount of ionic liquid absorbed into the polyimide struts, Equation 3 is employed. The compositions and densities used to calculate the scattering length densities for the polyimide and the three ionic liquid solvents can be found in Tables 2 and 5, respectively. The cylinder SLD is derived from the model fit of the neutron scattering curve. The volume fractions of solvent imbibed into the polyimide struts that result from this analysis are provided in Figures 10.

The dashed line on Figure 10 indicates the porosity of the polyimide aerogel struts. As described above, the aerogel struts have an inherent nano-porosity in addition to the macroscopic porous structures in the aerogel. When in a solvent environment, all of the polyimide struts contain solvent that is 25-50% larger than the porosity of the aerogel itself. Additionally, the cylinder radius of the aerogel is approximately 2-3 nm smaller than the solvated SE-Gels indicating that the process of solvent removal via supercritical drying (SCD-Gels) collapses the aerogel strut and possibly some of its pores.

Thus, this analysis clearly shows that the aerogel solvated with RTIL contains ionic liquid in the pores between struts, but also within the gel skeleton as well. The amount of ionic liquid in the struts varies with RTIL structure and size, suggesting that the partitioning of the RTIL in the strut can be controlled with polyimide aerogel and RTIL structure. Moreover, the presence of the RTIL within the strut will certainly impact its transport properties. Thus, the correlation of the performance of RTIL and polyimide aerogel constructs in functional applications to their hierarchical porosity and solvated composition is needed to more fully understand their structure-performance relationships.

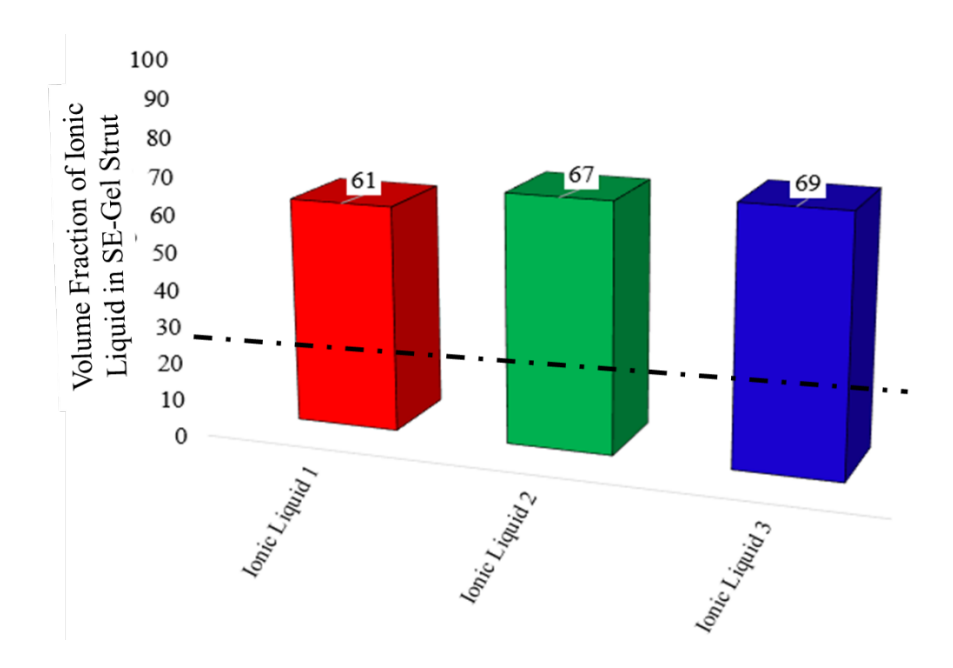


**Figure 10.** The volume fraction of ionic liquid in the Polyimide SE-Gel struts. The dashed line represents the porosity of the Polyimide Aerogel strut.

## **Conclusion:**

Small angle neutron scattering experiments provide insight into the size and composition of polyimide aerogel struts and the polyimide struts of gels saturated with various solvent environments. For the solvated gels, the introduction of solvent occurs via a solvent exchange (SE-

Gels) or after a super critical drying process (SCD-Gels). The size of the polyimide strut is reduced in aerogel form relative to when the gel becomes solvated, indicating that the polyimide strut collapses to some extent upon super-critical drying.

Careful analysis of the scattering intensity shows that the solvated skeletal strut is not pure polymer, which reveals that a hierarchical porosity exists among and within the struts of the polyimide aerogel. The porosity *in* the struts allows for solvent to imbibe the struts, where the polyimide struts can absorb up to ~ 70% ionic liquid and ~90% water/D<sub>2</sub>O. Approximately the same amount of water or D<sub>2</sub>O was absorbed into the struts. It is hypothesized that the differences in absorption within the struts between water and RTIL is dictated by the size, structure, and surface tension differences among all solvents tested. For ionic liquids, the amount of RTIL in the struts varies with RTIL structure, suggesting that the partitioning of the RTIL in the strut can be controlled with polyimide and RTIL structure. Moreover, the presence of the RTIL within the strut will certainly impact its transport properties. Additionally, the amount of solvent absorbed by the struts corresponds to a proportional increase in strut size.

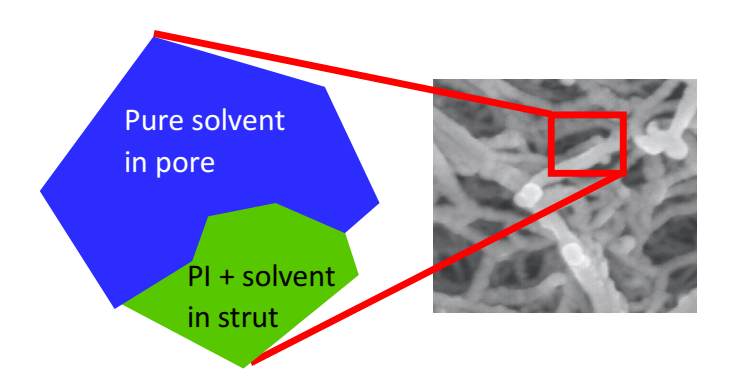
Commonly, characterization of aerogel systems has focused on the aerogels in the dry state, which emphasizes on the porosity and provides limited quantitative structural knowledge of the aerogel struts in functional applications. The results reported here provide insight into the existence of the hierarchy of nanopores in the polyimide, the solvated state of aerogel struts, and the influence super-critically drying plays in the nanostructure of the aerogel systems. The insight from these results, therefore, provides the foundation to investigate the further correlations between the nano- and mesoscale structural characteristics, fabrication processes, and the performance of polyimide aerogels and gel systems in functional applications such as polymeric battery separators.

#### **Acknowledgements:**

MDD acknowledges the support of the U.S. Department of Energy, Office of Science, Basic Energy Sciences, Materials Sciences and Engineering Division. SJR was supported by the National Science Foundation (DMR-1409034 and DMR-1808946). BNN, RPV, JW and MAM were supported by the Convergent Aeronautics Solutions (CAS) project under the NASA ARMD Transformative Aeronautics Concepts Program (TACP). MDD and MAM designed the experiments; MDD and SJR completed the scattering experiment, data analysis and interpretation; BNN, RPV synthesized and characterized the wet gel and aerogel samples; MDD and SJR led the writing of the manuscript, with input from MAM, RPV, JW and BNN. Heidi Guo, Linda McCorkle and Daniel A. Scheiman performed the BET surface area, SEM and TGA, respectively. A portion of this research used resources at the High Flux Isotope Reactor, a DOE Office of Science User Facility operated by the Oak Ridge National Laboratory. We acknowledge the support of the National Institute of Standards and Technology, U.S. Department of Commerce, in providing the neutron research facilities used in this work. Certain commercial equipment, instruments, or materials (or suppliers, or software) are identified in this paper to foster understanding. Such identification does not imply recommendation or endorsement by the National Institute of Standards and Technology, nor does it imply that the materials or equipment identified are necessarily the best available for the purpose.

This work benefited from the use of the SasView application, originally developed under NSF Award DMR-0520547. SasView also contains code developed with funding from the EU Horizon 2020 program under the SINE2020 project Grant No 654000.

# TOC Graphic:



#### **References:**

\_

- <sup>3</sup> Guo, H.; Meador, M.A.B.; McCorkle, L.; Quade, D.J.; Guo, J.; Hamilton, B.; Cakmak, M.; Sprowl, G.; **Polyimide Aerogels Cross-Linked Through Amine Functionalized Polyoligomeric Silsesquioxane** *ACS Appl Mater. Interfaces*, **2011**, *3*, 546-552.
- <sup>4</sup> Meador, M. A. B.; Wright, S.; Sandberg, A.; Nguyen, B. N.; Van Keuls, F. W.; Mueller, C. H.; Rodríguez-Solís, R. and Miranda, F. A.; **Low Dielectric Polyimide Aerogels as Substrates for Lightweight Patch Antennas** *ACS Appl. Mater. Interfaces*, **2012**, *4*, 6346-6353.
- <sup>5</sup> Mi, HY.; Jing, X.; Meador, M.A.B.; Guo, H.; Turng, LS.; Gong, S.; **Triboelectric Nanogenerators Made Of Porous Polyamide Nanofiber Mats And Polyimide Aerogel Film: Output Optimization And Performance In Circuits** *ACS Appl. Mater. Interfaces*, **2018**, *10*, 30596-30606.
- <sup>6</sup> Zhai, C.; Jana. S. C.; **Tuning Porous Networks in Polyimide Aerogels for Airborne Nanoparticle Filtration** ACS Appl. Mater. Interfaces, **2017**, *9*, 30074-30082
- <sup>7</sup> Guo, H.; Meador, M.A.B.; McCorkle, L.; Quade, D.J.; Guo, J.; Hamilton, B.; Cakmak, M. **Tailoring Properties Of Cross-Linked Polyimide Aerogels For Better Moisture Resistance, Flexibility, And Strength** *ACS Appl. Mater. Interfaces*, **2012**, *4*, 5422-5429.
- <sup>8</sup> Pantoja, M.; Boynton, N.; Cavicchi, K. A.; Dosa, B.; Cashman, J. L.; Meador, M. A. B.; **Increased Flexibility in Polyimide Aerogels using Aliphatic Spaces in the Polymer Backbone** *ACS Appl. Mater. Interfaces,* **2019,** *11*, 9425-9437.
- <sup>9</sup> Vivod, S.L.; Meador, M.A.B.; Pugh, C.; Wilkosz, M.; Calomino, K.; McCorkle, L;. **Toward Improved Optical Transparency of Polyimide Aerogels** ACS *Appl. Mater. Interfaces*, **2020**, *12* (7), 8622-8633.
- <sup>10</sup> Meador, M. A. B.; Malow, E.; Silva, R.; Wright, S.; Quade, D.; Vivod, S. L.; Guo, H.; Guo, J.; Cakmak, M.; **Mechanically Strong, Flexible Polyimide Aerogels Cross-Linked with Aromatic Triamine** *ACS Appl. Mater. Interfaces*, **2012**, *4*, 536-544.
- <sup>11</sup> Kawagishi, K.; Saito, H.; Furukawa, H.; Horie, K.; **Superior Nanoporous Polyimides via Supercritical CO<sub>2</sub> Drying of Jungle-Gym-Type Polyimide Gels** *Macromol. Rapid Commun.*, **2007**, 28, 96-100.
- <sup>12</sup> Guo, H.; Meador, M. A. B.; McCorkle, L; Quade D. J.; Guo, J.; Hamilton, B.; Cakmak, M.; Sprowl, G;. **Polyimide Aerogels Cross-Linked through Amine Functionalized Polyoligomeric Silsesquioxane** *ACS Appl. Mater. Interfaces*, **2011**, *3*, 546-552

<sup>&</sup>lt;sup>1</sup> Meador, M.A.B.; McMillon, E.; Sandberg, A.; Barrios, E.; Wilmoth, N.G.; Mueller, C.H.; Miranda, F.A.; **Dielectric And Other Properties Of Polyimide Aerogels Containing Fluorinated Blocks** *ACS Appl. Mater. Interfaces*, **2014**, *6*, 6062-6068.

<sup>&</sup>lt;sup>2</sup> Del Corso, J. A.; Cheatwood, F. M.; Bruce, W. E.; Hughes, S. J.; Calomino, A. M. **21**<sup>st</sup> **AIAA Aerogynamic Decelerator Systems Technology Conference and Seminar**; Dublin Ireland, May 23-26, 2011; AIAA: Reston, VA. 2011; 2510.

<sup>13</sup> Meador, M.A.B.; Alemán, C.R.; Hanson, K.; Ramirez, N.; Vivod, S.L.; Wilmoth, N.; McCorkle, L.; **Polyimide Aerogels With Amide Cross-Links: A Low Cost Alternative For Mechanically Strong Polymer Aerogels** *ACS Appl. Mater. Interfaces*, **2015**, *7*, 1240-1249.

- <sup>14</sup> Nguyen, B.N.; Meador, M.A.B.; Scheiman, D.; McCorkle, L.; **Polyimide Aerogels Using Triisocyanate As Cross-Linker** *ACS Appl. Mater. Interfaces*, **2017**, *9*, 27313-27321.
- <sup>15</sup> Lutkenhaus, J. L.; McEnnis, K.; Hammond, P. T.; **Nano- and Microporous Layer-by-Layer Assemblies Containing Linear Poly(ethylenimine) and (Poly(acrylic acid)** *Macromolecules*, **2008**, *41*, 6047-6054.
- <sup>16</sup> Tigelaar, D.M.; Meador, M.A.B.; Kinder, J.D.; Bennett, W.R.; **New APTES Cross-Linked Polymers From Poly(Ethylene Oxide) S And Cyanuric Chloride For Lithium Batteries** *Macromolecules*, **2006**, *39*, 120-127.
- <sup>17</sup> Tigelaar, D.M.; Meador, M.A.B.; Bennett, W.R.; Composite Electrolytes For Lithium Batteries: Ionic Liquids In APTES Cross-Linked Polymers *Macromolecules*, **2007**, *40*, 4159-4164.
- <sup>18</sup> Tigelaar, D.M.; Palker, A.E.; Meador, M.A.B.; Bennett, W.R.; **Synthesis And Compatibility Of Ionic Liquid Containing Rod-Coil Polyimide Gel Electrolytes With Lithium Metal Electrodes** *Journal of the Electrochemical Society*, **2008**, *155*, A768-A774.
- <sup>19</sup> Hapiot, P.; Lagrost, C.; **Electrochemical Reactivity in Room-Temperature Ionic Liquids** *Chemical Reviews*, **2008**, *108*, 2238-2264.
- <sup>20</sup> Hapiot, P.; Lagrost, C.; **Electrochemical Reactivity in Room-Temperature Ionic Liquids** *Chem. Rev.*, **2008**, *108*, 2238-2264.
- <sup>21</sup> Zhang, S.; Sun, N.; He, X.; Lu, X.; Zhang, X.; **Physical Properties of Ionic Liquids: Database and Evaluation** *Journal of Physical and Chemical Reference Data*, **2006**, *35*, 1475-1517.
- <sup>22</sup> Every, H. A.; Bishop, A. G.; Forsyth, M.; MacFarlane, D.; **Ion Diffusion In Molten Salt Mixtures** *Electrochimica Acta*, **2000**, *45*, 1279-1284.
- <sup>23</sup> Feigin, L. A.; Svergun, D. I.; **Structure Analysis by Small-Angle X-Ray and Neutron Scattering** Plenum Press, NY. A Division of Plenum Publishing Corporation,
- <sup>24</sup> Radlinski, A. P.; Mastalerz, M.; Hinde, A. L.; Hainbuchner, M.; Rauch, H.; **Application of SAXS and SANS in Evaluation of Porosity, Pore Size Distribution and Surface Area of Coal** *International J. of Coal Geology*, **2004**, *59* (*3-4*), 245–271.
- <sup>25</sup> Pan, J.; Niu, Q.; Wang, K.; Shi, X.; Li, M.; **The Closed Pores of Tectonically Deformed Coal Studied by Small-Angle X-Ray Scattering and Liquid Nitrogen Adsorption Microporous Mesoporous Materials** *Energy Fuels*, **2016**, 224, 245–252.
- <sup>26</sup> Deshpande, S.; Kulkarni, A.; Sampath, S.; Herman, H.; **Application of Image Analysis for Characterization of Porosity in Thermal Spray Coatings and Correlation with Small Angle Neutron Scattering** *Surface and Coating Tech*; **2004**, *187* (1), 6–16.
- <sup>27</sup> He, L.; Melnichenko, Y. B.; Mastalerz, M.; Sakurovs, R.; Radlinski, A. P.; Blach, T.; **Pore Accessibility by Methane and Carbon Dioxide in Coal as Determined by Neutron Scattering** *Energy Fuels*, **2012**, *26*, *1975-1983*.

<sup>28</sup> Hall, P. J.; Machado, W. R.; Galan, D. G.; Barria, E. B.; Sherrington, D. C.; **Use of Contrast Matching Small-Angle Neutron Scattering to Monitor the Presence of Closed Porosity in Controlled Porosity Styrendivinylbenzene Resins** *Faraday*, **1996**, *92* (14), 2607–2610.

- <sup>29</sup> Lopez-Rubio, A.; Paul, E.; **Neutron Scattering: A Natural Tool for Food Science and Technology Research** *Trends in Food Sci. Technol.*, **2009**, *20*, 576–586.
- <sup>30</sup> Crawshaw, J.; Vickers, M. E.; Briggs, N. P.; Heenan, R. K.; Cameron, R. E.; **The Hydration of TENCEL Cellulose Fibres Studied Using Contrast Variation in Small Angle Neutron Scattering** *Polymer*, **2000**, *41*, 1873–1881.
- <sup>31</sup> Shibayama, M.; Nagao, M.; Okabe, S.; Karino, T.; **Evaluation of Incoherent Neutron Scattering from Softmatter** *J. Phys. Soc. Japan*, **2005**, *74* (10), 2728–2736.
- <sup>32</sup> Guinier, A.; Fournet, G.; Small Angle Scattering of X-Rays; Mayer, M. G., Ed.; John Wiley & Sons, Inc.: London, **1955**.
- <sup>33</sup> Calo, J. M.; Hall, P. J.; **The Application of Small Angle Scattering Techniques to Porosity Characterization in Carbons**. *Carbon*, **2004**, *42*, 1299–1304.
- <sup>34</sup> Fischer, S.; Hartl, C.; Frank, K.; Ra, J. O.; Liedl, T.; Nickel, B.; **Shape and Interhelical Spacing of DNA Origami Nanostructures Studied by Small-Angle X Ray Scattering** *Nanolett.*, **2016**, *16*, 4282-4287.
- <sup>35</sup> Hedden, R. C.; Lee, H.; Bauer, B. J.; Characterization of Nanoporous Low- k Thin Films by Small-Angle Neutron Scattering Contrast Variation *Langmuir*, 2004, 416–422.
- <sup>36</sup> Jiang, M.; Li, H.; Zhou, L.; Xing, R.; Zhang, J.; **Hierarchically Porous Graphene/ZIF 8 Hybrid Aerogel: Preparation, CO 2 Uptake Capacity, and Mechanical Property** *ACS Appl. Mater. & Interfaces*, **2018**, *10*, 827-834.
- <sup>37</sup> Hao, P.; Zhao, Z.; Tian, J.; Li, H.; Sang, Y.; Yu, G.; Cai, H.; Liu, H.; Wong, C. P.; Umar, A.; **Hierarchical Porous Carbon Aerogel Derived from Bagasse for High Performance Supercapacitor** *Nanoscale*, **2014**, *6*(20), 12120–12129.
- <sup>38</sup> Ren, L.; Hui, K. N.; Hui, K. S.; Liu, Y.; Qi, X.; Zhong, J.; Du, Y.; **3D Hierarchical Porous** Graphene Aerogel with Tunable Meso-Pores on Graphene Nanosheets for High-Performance Energy Storage *Scientific Reports*, **2015**, *5*, 1–11.